ACCSCIENCE PUBLISHING

Materials Science in Additive Manufacturing

ORIGINAL RESEARCH ARTICLE

Numerical and experimental assessment of non-monolithic fabrication effects on sound transmission and absorption in additively manufactured metamaterials

Supplementary File

S1. Computer-aided design dimensions and mesh independence analysis

Table S1 provides the detailed information about the perforation diameter for each layer. It may be noted that the orientation of the rectangular perforation differs between D15 and D18; this was done to ensure that the perforation does not decimate the underlying auxetic material. Figure S1 shows the side profile of both designs investigated in this study, where Figure S1a shows D15 and Figure S1b shows D18. Each layer height can be clearly identified. Figure S2 is color-coded in the same manner as Figure S1 for ease of understanding. Figure S2 shows the clear location of each perforation, which is center-aligned with the auxetic cavity. Figure S3 provides details on the effects of different meshing schemes for micro-perforations. Figure S3a shows the computer-aided design (CAD) model created in SolidWorks, while Figure S3b shows the numerical model prepared in COMSOL with an air domain at the top. Mesh independence was investigated in two steps, first by decreasing the smallest element size to $2.7e^{-5}$ mm and the largest element size to 1/7 of the largest analyzed frequency. Secondly, by creating a boundary layer mesh in the perforations (Figure S3c-1) and a fine mesh without boundary layers (Figure S3c-2). Results are shown in Figure S3d, where it is evident that the literature-defined limits are sufficient to accurately predict the sound absorption coefficient (SAC). 70,703 elements represent the mesh at literature-recommended settings, 110,018 elements represent a fine mesh without boundary layers, and 193,811 elements represent a fine mesh with boundary layers in the perforated regions. As the boundary layer mesh had no effect with the refined meshing in place inside the perforations, all subsequent meshes were kept refined, but without boundary layers to save computational power. Figure S3e compares the numerical model with 70,703 elements to the data from the referenced literature.

As in the case of SAC, an in-depth mesh-independence study was also conducted to ensure numerical model accuracy. Figure S4a shows the model used for analysis; Figure S4b shows the domains and associated physics; and Figure S4c-1 and S4c-2 show the thermoviscous acoustics domain with and without boundary layers, respectively. In Figure S4d, the mesh independence is shown; note that the element sizes were kept the same as in the SAC case. Meanwhile, 86,311 elements represent the minimum element size requirement as defined in the preceding paragraph, 188,280 elements represent the refined mesh, and 192,433 elements represent the boundary layers created within the thermoviscous acoustics domain. As evident, the minimum requirements for accurate sound transmission loss (STL) are met without creating boundary layers or requiring further mesh refinement; therefore, all subsequent analyses ensured that the element size was small enough to accurately capture the STL. Thus, limiting the computational load. Figure S4e compares results from the literature with those from our numerical model. This comparison is presented with an 86,311-element numerical model.

Table S1. Layer-wise perforation measurements for both designs (all dimensions in mm)

Design	Top layer	1st layer	2nd layer	3rd layer
D15	2.75 × 7 rectangle	3.75, 3.5, 3.25, 3, 2.75, 2.5, r	2.25, 2, 1.75, 1.5, 1.25, 1, r	15 × 0.75 holes per auxetic
D18	5 × 2 rectangle		2 rows of 2.25, 2, 1.75, 1.5, 1.25, 1, r	

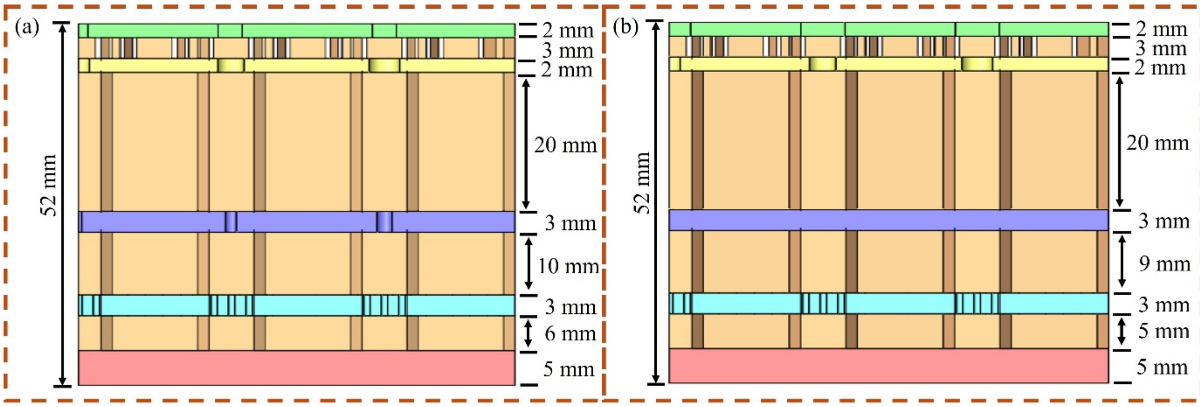

Figure S1. Side profiles for the height of each layer. (a) D15. (b) D18.

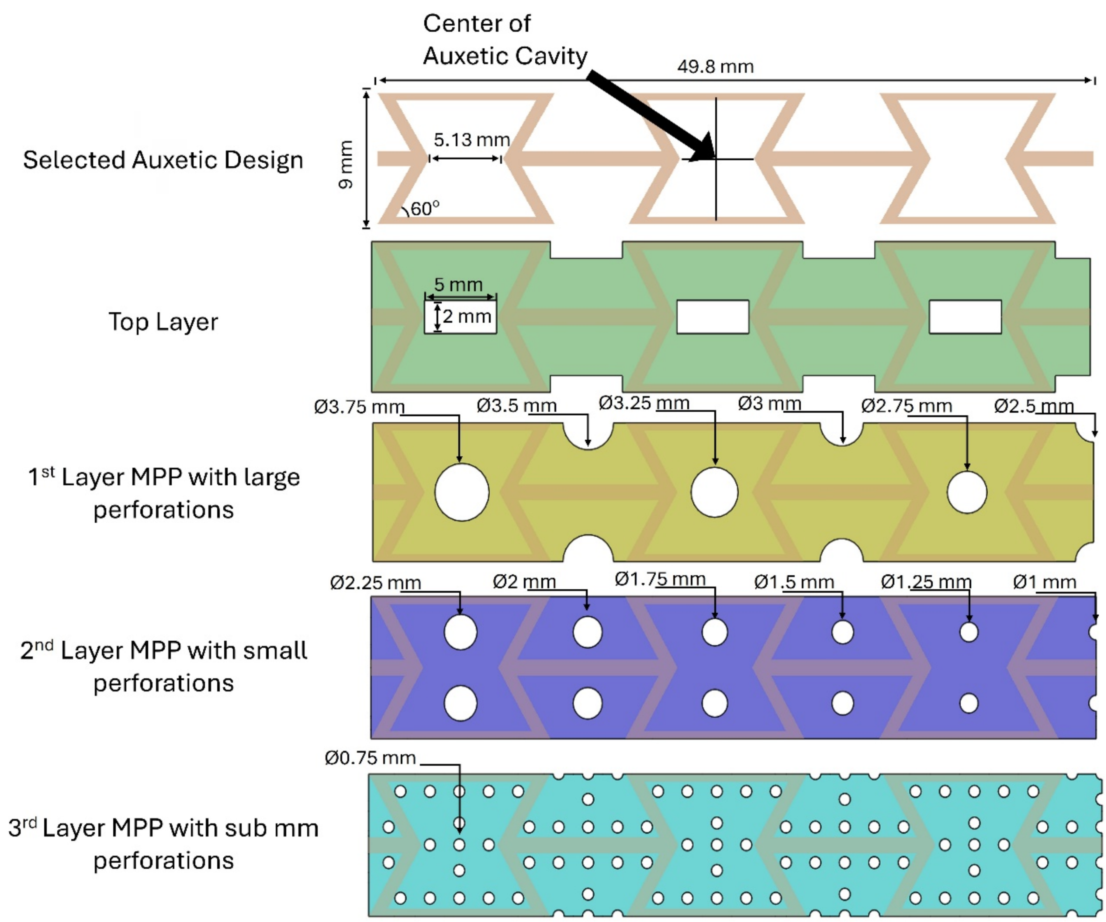

Figure S2. Perforation location in design D18
Abbreviation: MPP: Micro-perforated plate.

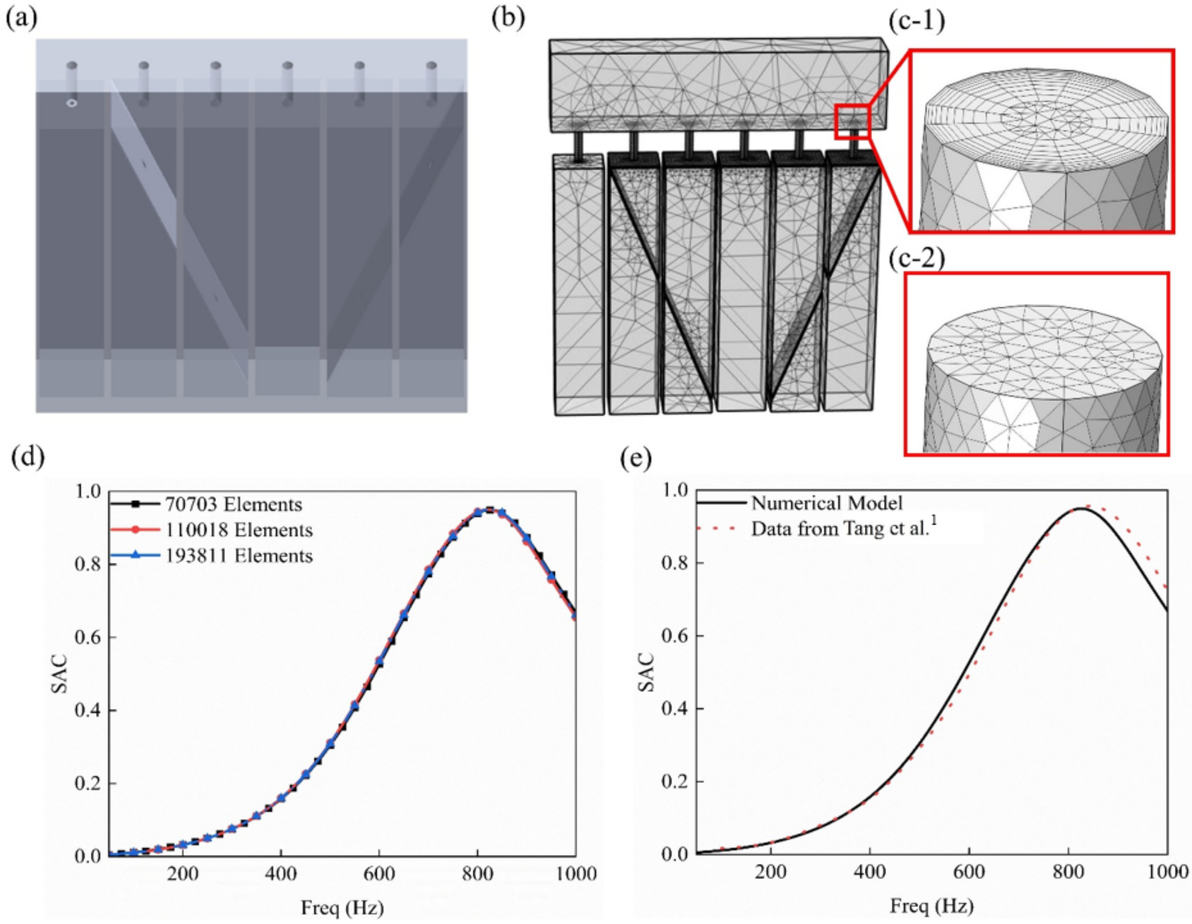

Figure S3. Numerical model validation for sound absorption coefficient (SAC). (a) Computer-aided design (CAD) model built in SolidWorks. (b) Numerical model in COMSOL. (c-1) Boundary layer mesh in perforations. (c-2) Refined mesh without boundary layer in perforations. (d) Numerical model comparison for different mesh settings. (e) Numerical model results vs. results from literature.

S2. Parameter settings for additive manufacturing technologies

Table S2 provides details of the print parameters used for fused deposition modeling (FDM)-manufactured designs. For stereolithography (SLA) and selective laser sintering (SLS), original equipment manufacturer (OEM)-recommended print parameter settings were utilized. Tables S3 and S4 list these details. Table S5 lists the parameter settings utilized for digital light processing (DLP) manufacturing. It must be noted that the SLA and SLS equipment used in this research has built-in parameter settings for each material/resin. No modifications were performed to default settings; however, for ease of understanding and reproducibility, settings for parameters that can be modified are being shared.

Table S2. Print parameters for fused deposition modeling

Parameter	Setting
Nozzle diameter	0.4 mm
Layer height	0.2 mm
Infill density	100%
Nozzle temperature	230 °C
Bed temperature	60 °C
Chamber temperature	50 °C
Print speed	50 mm/s
Retraction speed	40 mm/s
Retraction length	2 mm

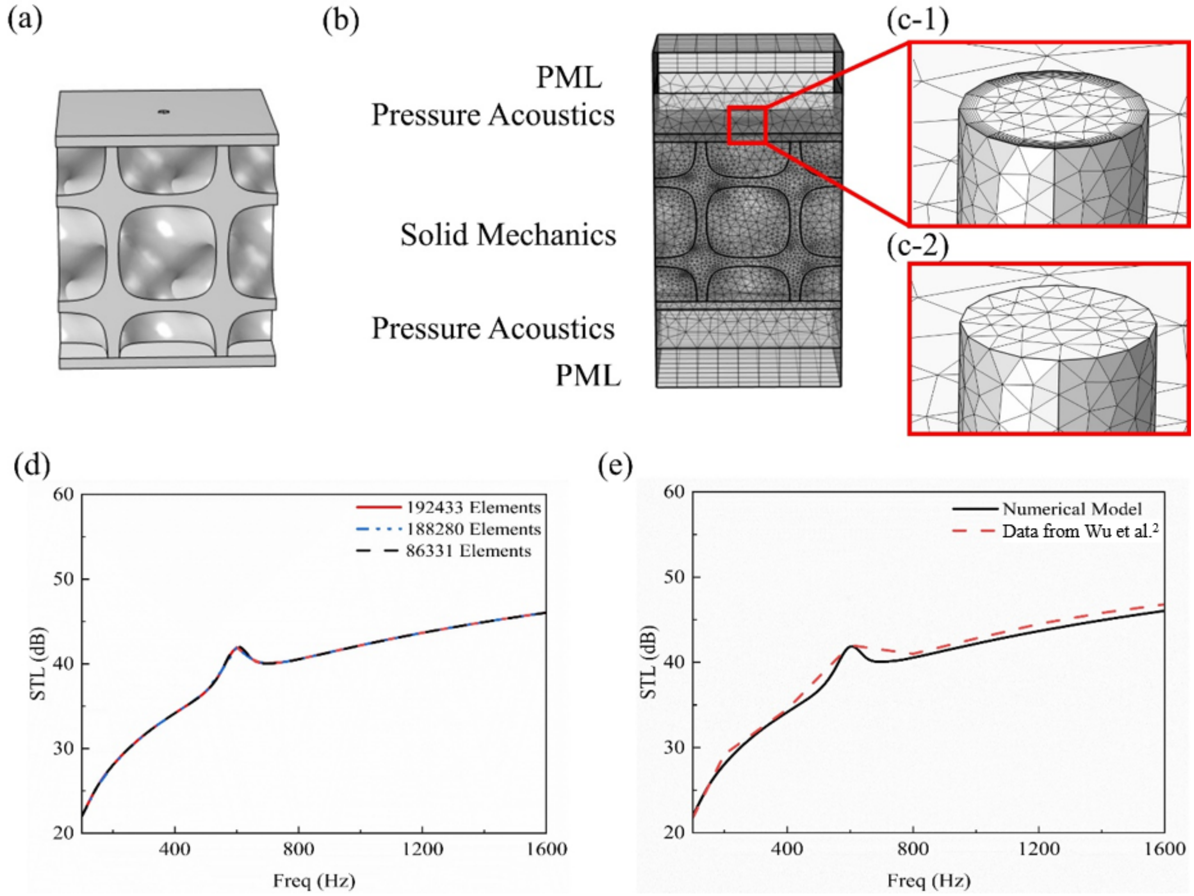

Figure S4. Numerical model validation for sound transmission loss (STL). (a) Numerical model in COMSOL. (b) Mesh with domain physics representation (c-1) Boundary layer mesh in perforation. (c-2) Refined mesh without boundary layer in perforation. (d) Numerical model comparison for different mesh settings. (e) Numerical model results vs. results from literature.

Table S3. Print parameters for stereolithography

Parameter	Setting
Layer thickness	0.1 mm
Raft type	Full raft
Raft thickness	1.5 mm
Height above raft	5 mm
Support type	Touch
Touchpoint size	0.25 mm

Table S4. Print parameters for selective laser sintering

Parameter	Setting
Layer thickness	0.1 mm
Laser power	21 W
Laser speed	2,500 mm/s
Hatch distance	0.25 mm
Infill	On
Upskin	On
Downskin	On

Table S5. Print parameters for digital light processing

Parameter	Recommended	Modified	Target layer
Layer height	0.05 mm	–	
Lifting distance	8 mm	–	
Lifting speed	60 mm/min	–	All
Retract distance	8 mm	–	
Retract speed	150 mm/min	–	
Layers count	6	–	Base
Exposure time	40 s	70 s	
Transition layers count	6	–	Support
Exposure time	8.5 s	10.5 s	Other

S3. Microscopic defect analysis

Figure S5 shows the images of qualitative microscopic analysis, where Figure S5a–c show the DLP-manufactured design D18 and Figure S5d–f show the SLS-manufactured design D18. The features were much more refined in DLP than SLS, as microparticles were observed at the corners of small features and perforations. These particles made edges round and perforations distorted, as shown in Figure S5d and S5e, whereas Figure S5a and S5b show sharp, defined edges for the manufactured samples. Comparison of Figure S5c and S5f further demonstrates the superiority of DLP, as several 0.75 mm perforations were closed in SLS-manufactured parts. On the other hand, Figure S6 shows a quantitative analysis in which both processes accurately manufactured a 0.75 mm perforation diameter.

S4. Further analysis

Figure S7 depicts the segregation of incoming sound energy upon interaction with any surface in its path. Table S6 provides a comparison of overall height for the designs prepared from all the technologies used in this study. The designed height of both designs was 52 mm. FDM and SLA had the closest heights to the designed value due to monolithic fabrication. While attempts were made to ensure the subassemblies fit seamlessly, micro-gaps remained, resulting in sound energy leakage and an increased overall height of the design.

Table S7 presents the measured dimensions of spacers manufactured via SLA to investigate the STL observed in assembled samples. Average values reported in the table were measured using a digital vernier calliper. The spacers were designed to maintain a gap of approximately 2 mm between the layers. However, their actual thickness was found to be less than 2 mm due to shrinking. In the slicer, the model was oriented so that the support structures were not generated on the sides intended to be bonded to the surface, to ensure consistent thickness.

Figure S8 presents the effect of introducing a 2 mm gap between layers in the D18 design, both experimentally and numerically. It was observed that the STL deteriorated considerably in both instances, further supporting the finding that interstitial leakages are the major contributor to STL deviation. The differences between numerical and experimental data stemmed from manufacturing defects and clogging of perforations observed during microscopic analysis. At lower frequencies, the difference was considerable, as thermoviscous losses were significantly higher than at higher frequencies.

Table S6. Overall dimensions of the manufactured designs

Technology	D15 (mm)	D18 (mm)
FDM	51.92	52.04
SLA	52.35	52.09
DLP	53.86	53.14
SLS	53.84	51.87

Abbreviations: DLP: Digital light processing; FDM: Fused deposition modeling; SLA: Stereolithography; SLS: Selective laser sintering.

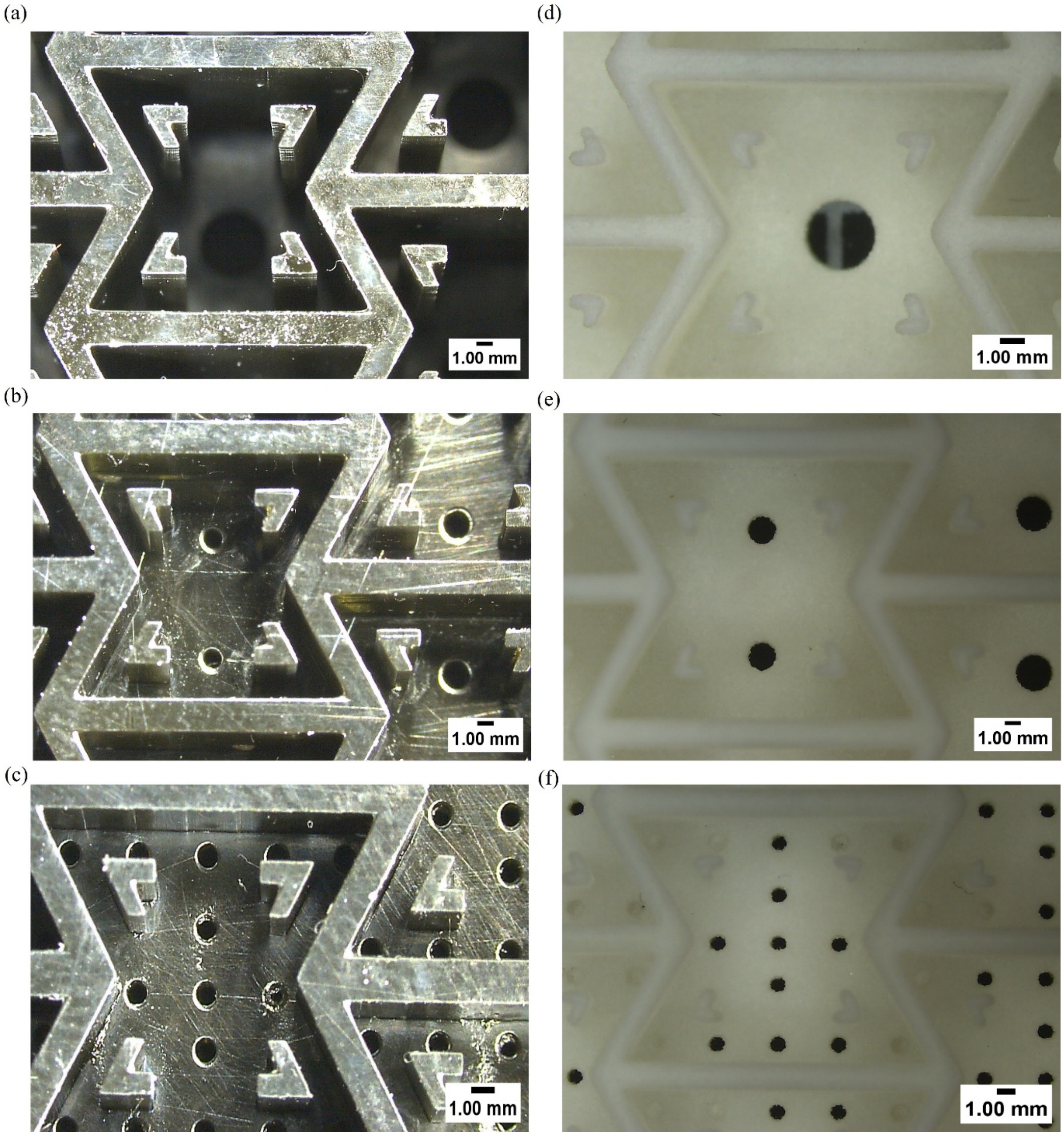

Figure S5. Qualitative microscopic analysis for identifying defects. (a) Supports and auxetics created by digital light processing (DLP). (b) 1 mm perforation created by DLP. (c) 0.75 mm perforations manufactured by DLP. (d) Supports and auxetics created by selective laser sintering (SLS). (e) 1 mm perforation created by SLS. (f) 0.75 mm perforations manufactured by SLS, with several perforations clogged with agglomerated powder. Scale bars: 1 mm.

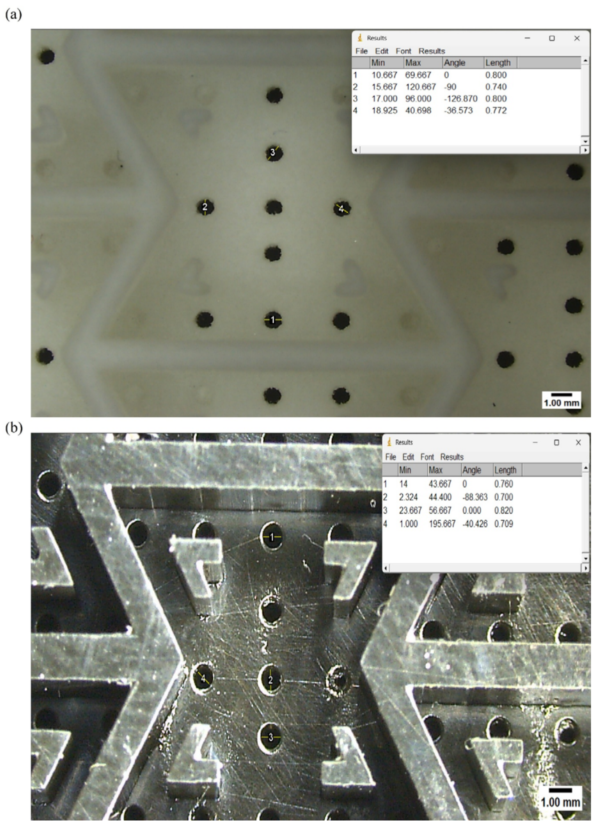

Figure S6. Quantitative comparison of the smallest perforations manufactured with different additive manufacturing technologies. (a) Selective laser sintering. (b) Digital light processing. Scale bars: 1 mm.

Table S7. Average thickness of the manufactured spacers

Spacer	Dimension (mm)
1	1.91
2	1.91
3	1.91
4	1.91
5	1.91
6	1.90
7	1.91
8	1.90
9	1.91
10	1.91
11	1.90
12	1.91
13	1.91
14	1.90
15	1.91
16	1.91
17	1.91
18	1.87
19	1.92
20	1.90

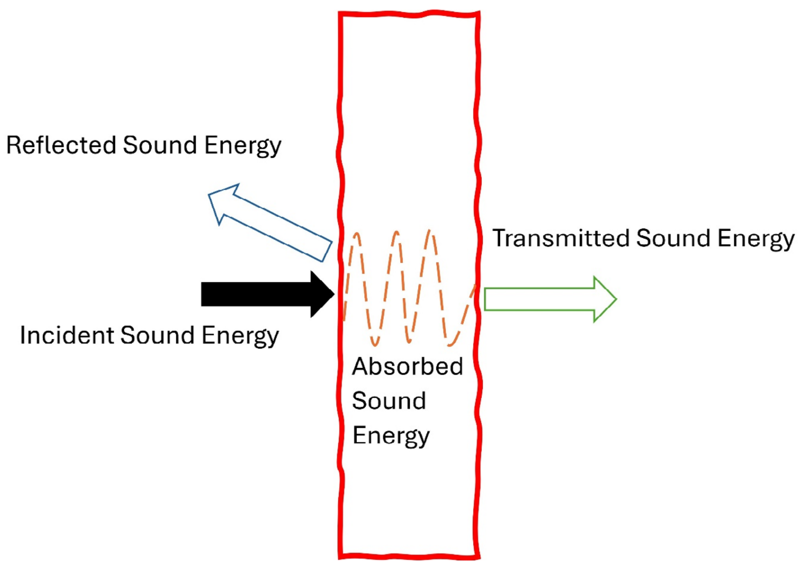

Figure S7. Schematic representation of acoustic energy distribution at a material interface, illustrating incident, reflected, absorbed, and transmitted components

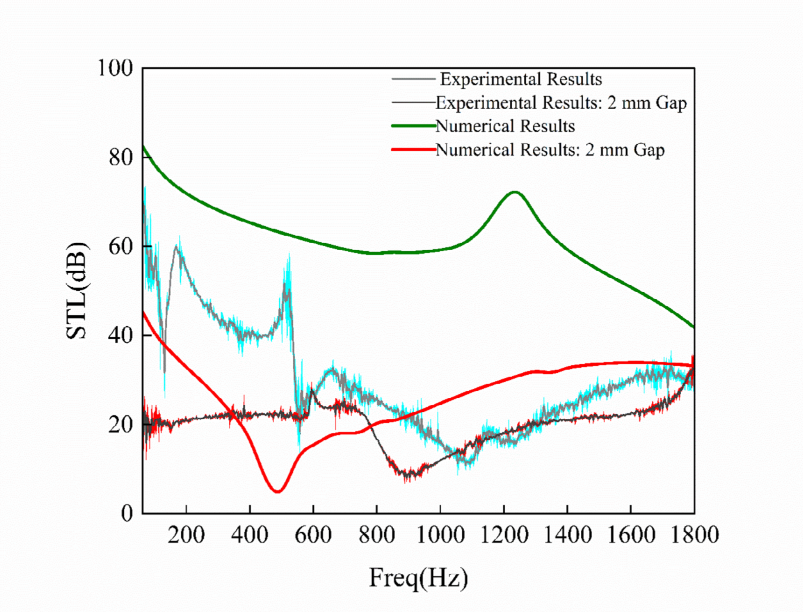

Figure S8. Effect of introducing a gap in numerical and experimental results
Abbreviations: Freq: Frequency; STL: Sound transmission loss.

References

1. Tang Y, Ren S, Meng H, *et al*. Hybrid acoustic metamaterial as super absorber for broadband low-frequency sound. *Sci Rep*. 2017;7(1):43340.

   doi: 10.1038/srep43340

2. Wu Y, Qi X, Sun L, Wang B, Wang P, Li W. Acoustic Performance of Micro-Perforated Plate Sandwich Structure Based on Triply Periodic Minimal Surfaces. *Mater Today Commun*. 2025;49:114249.

   doi: 10.1016/j.mtcomm.2025.114249